

Native point defects in yttria as a high-dielectric-constant gate oxide material: a first-principles study

J.X. ZHENG¹, G. CEDER^{1,2}, T. MAXISCH², W.K. CHIM^{1,3} and W.K. CHOI^{1,3}

¹Singapore-MIT Alliance, 4 Engineering Drive 3, Singapore 117576

²Massachusetts Institute of Technology, 77 Massachusetts Avenue, Cambridge, MA 02139-66307, USA

³Department of Electrical & Computer Engineering, National University of Singapore, 4 Engineering Drive 3, Singapore 117576

Abstract--Yttria (Y_2O_3) has become a promising gate oxide material to replace silicon dioxide in metal-oxide-semiconductor (MOS) devices. The characterization of native point defect in Y_2O_3 is essential to understand the behavior of the material. We used the first-principles pseudopotential method to study the electronic structure, defect structure and formation energy of native point defects in Y_2O_3 . Vacancies, interstitials and antisites in their relevant charge states are considered. The dominant defect types are identified under different chemical potentials and different Fermi levels. Oxygen vacancies are the dominant defect types under high yttrium chemical potential condition. Lower yttrium chemical potential leads to oxygen interstitials and ultimately yttrium vacancies when Y_2O_3 is used as a high dielectric constant gate oxide material in MOS devices.

I. INTRODUCTION

Yttrium oxide (Y_2O_3) is widely used in ceramic and glass applications as it has a high melting point, and presents a high breakdown field strength, good chemical stability, and low expansion characteristics to glass. Y_2O_3 is also an important oxide-based phosphor material and is used as a host material in rare-earth-doped lasers. Recently Y_2O_3 has also received attention as a promising candidate for replacing silicon dioxide (SiO_2) as a gate dielectric material in metal-oxide-semiconductor (MOS) transistors [1-10].

The continual scaling of complementary MOS technologies has pushed SiO_2 gate oxide to its minimal thickness limit. Extensive research efforts have focused on finding a suitable high-k oxide material to replace SiO_2 as a gate dielectric. Y_2O_3 has emerged as a promising candidate as it has a moderately high dielectric constant (~16),

relatively high band offsets with respect to silicon, and exhibits thermodynamic stability in contact with silicon (Si). Y_2O_3 is also one of the few high dielectric constant (high-k) oxides that is epitaxially matched to Si, as its lattice constant (10.6 Å) is about two times that of Si (5.43 Å). This property of Y_2O_3 suggests that a sharp Y_2O_3 /Si interface with low interface trap density can potentially be obtained.

Although many experimental groups have studied the structural and electrical properties of the Y_2O_3 /Si system [4-10], epitaxial Y_2O_3 film still does not have good structural and electrical quality. One major problem is the poor electrical characteristics of the interface between the high-k dielectric and the Si substrate. Another problem is the high density of pre-existing defects in the dielectric. These defects generate positive fixed charge which shift the flatband voltage, and electron traps which cause threshold voltage instabilities [8-10].

The structural and electronic properties of stoichiometric Y_2O_3 have been studied theoretically in Refs. [11-14] and the effect of neutral oxygen vacancies on the electronic structure of Y_2O_3 was investigated by Jollet *et al.* [12]. However, a detailed theoretical study of the intrinsic point defects in Y_2O_3 is lacking. In this study, we attempt to understand the native point defects in bulk yttria through first-principles calculation by calculating the formation energy of various point defects as a function of Fermi level and yttrium (Y) or oxygen (O) chemical potentials.

II. COMPUTATIONAL METHODOLOGY

A. Methodology

Calculations have been performed using the generalized gradient approximation (GGA) with the Perdew-Wang exchange correlation

within the framework of density functional theory (DFT), as implemented in the VASP (Vienna *ab-initio* simulation package) code [15]. Projector augmented wave (PAW) pseudopotentials [16] are generated in the configuration of $4s^2 4p^6 5s^2 4d^1$ for the valence electrons in the yttrium atom and in the configuration of $2s^2 2p^4$ for the valence electrons in the oxygen atom. The primitive cell of Y_2O_3 consists of 40 atoms, but a cubic bixbyite structure with 80 atoms is used to compute defect states. There are two inequivalent cation sites, Y1 at the $8b$ site (at position $(\frac{1}{4}, \frac{1}{4}, \frac{1}{4})$) and Y2 at the $24d$ site (at position $(u, 0, \frac{1}{4})$), and one type of O at the $48e$ site (at position (x, y, z)). The structure is defined by the lattice parameter a and by the four internal structural parameters u , x , y , and z .

The formation energy of point defects that do not preserve the Y_2O_3 stoichiometry depends on the external chemical potentials. We follow the standard formalism outlined in several previous papers [17-23] to define reasonable bounds on the chemical potentials and to investigate the defect energies within these limits. The Y and O chemical potentials are not independent but related to the total energy of Y_2O_3 :

$$2\mu_Y^{Y_2O_3} + 3\mu_O^{Y_2O_3} = E_{Y_2O_3} \quad (1)$$

where $\mu_Y^{Y_2O_3}$ and $\mu_O^{Y_2O_3}$ are the chemical potential of Y and O in Y_2O_3 respectively, and $E_{Y_2O_3}$ is the energy per molecule of pure Y_2O_3 . The Y_2O_3 compound can exist within a range of oxygen and yttrium chemical potentials, defined by the competing phases at other Y/O ratios. The largest possible range for μ_O and μ_Y is obtained from the stability limits of Y_2O_3 with respect to metallic yttrium and molecular oxygen. To prevent pure Y formation, the following condition needs to be fulfilled:

$$\mu_Y^{Y_2O_3} < \mu_Y^o \quad (2)$$

where $\mu_Y^{Y_2O_3}$ is the chemical potential of Y in Y_2O_3 and μ_Y^o is the chemical potential of Y in pure yttrium metal. To prevent oxygen loss, the following condition needs to be fulfilled:

$$\mu_O^{Y_2O_3} < \mu_O^o \quad (3)$$

where $\mu_O^{Y_2O_3}$ is the chemical potential of O in Y_2O_3 and μ_O^o is the energy of pure O_2 gas (per oxygen atom). These chemical potentials are related by the formation energy of Y_2O_3 from metallic Y and O_2 gas:

$$\Delta E_f^{Y_2O_3} = 2\mu_Y^{Y_2O_3} - 2\mu_Y^o + 3\mu_O^{Y_2O_3} - 3\mu_O^o \quad (4)$$

Combining Eqs. (2), (3), and (4), we obtain the range of $\mu_Y^{Y_2O_3}$ for which the defect energies should be evaluated:

$$\mu_Y^o + \frac{1}{2}\Delta E_f^{Y_2O_3} < \mu_Y^{Y_2O_3} < \mu_Y^o \quad (5)$$

The range for $\mu_O^{Y_2O_3}$ can be found by combining Eqs. (1) and (5).

B. Defect formation energies

The supercell approach is used to calculate defect energies in this study. A defect α in charge state q is placed in a large Y_2O_3 supercell which is repeated periodically. To calculate the formation energy of charge states, a neutralizing background charge is applied. The formation energy (E_f) of a charged point defect [α^q] in Y_2O_3 is computed as

$$E_f[\alpha^q] = E[\alpha^q] \pm \mu_X - E[bulk] + q(E_V + \Delta V + \epsilon_F) \quad (6)$$

where $E[\alpha^q]$ is the total energy of a supercell containing a point defect α with charge q , μ_X is the external chemical potential of element X with + sign for vacancy and - sign for interstitial defect, $E[bulk]$ is the total energy of a perfect supercell, and E_V is the valence band maximum (VBM) in the perfect supercell. The Fermi level is taken as the energy of the electron reservoir (electron chemical potential μ_c) from (in) which an electron is removed (placed) to form a charged defect. The Fermi level is conventionally taken to be zero at the VBM of the perfect supercell. Because the valence band is displaced in calculations on small supercells with defects, its value needs to be referenced back to the valence band in the perfect crystal by an amount ΔV [19-23]. The shift of the VBM in supercell calculations, ΔV , can be obtained from the difference between the average potential in a bulk-like environment of the defect supercell and the average potential in the perfect bulk supercell. To calculate the average potential, the macroscopic averaging technique [24-25] is used to find the shift in the VBM. The three-dimensional electrostatic potential is reduced to a one-dimensional planar average first, and the macroscopic average of electrostatic potential is calculated over the primitive cell along one direction.

For charged systems, the energy of charged defects converges very slowly with supercell size due to electrostatic interactions

between the defects across the periodic boundary conditions. This interaction scales as $1/\epsilon L$ where L is the linear dimension of the supercell and ϵ is the dielectric constant [26]. To achieve faster convergence, Makov and Payne [26] suggested adding correction terms to the energy to account for defect-defect interactions induced by the periodic boundary conditions. Although this approach works well for atomic or molecular systems, it may lead to an overestimation of the correction term for defects in semiconductors due to the increased screening from valence electrons which effectively reduce the strength of the interactions [23, 27, 28]. For this reason, we have not included these correction terms in this study.

Errors in the defect formation energy can come from various sources. Well-converged calculations reduce the error from plane-wave energy cutoff and k -point sampling below 10 meV. The interaction between charged defects can introduce an error on the order of 0.1 eV and this error may become larger for higher-charged defects. The band gap error due to density-functional theory itself would have a significant effect on donor-like defects and is discussed with more details in Sec. IV. In summary, an error for defect formation energies of at least a few tenths of eV should always be assumed.

The thermodynamic transition between two charge states on the defect q_1 and q_2 occurs for the Fermi level at which the formation energy

of $[q_1]$ is equal to that of $[q_2]$, i.e., $E_f[q_1] = E_f[q_2]$. Using Eq. (6), it can be shown that the thermodynamic transition level q_1/q_2 is

$$\varepsilon_F[q_1/q_2] = \frac{1}{q_2 - q_1} (E[q_1] - E[q_2] + q_1(E_V + \Delta V_1) - q_2(E_V + \Delta V_2)) \quad (7)$$

where q_1 and q_2 are the initial and final charge states respectively (including the signs), ΔV_1 and ΔV_2 are the VBM shift for the initial and final charge states respectively, and $\varepsilon_F[q_1/q_2]$ is the Fermi energy level at which the transition from q_1 to q_2 takes place. This thermodynamic transition level can be directly observed in deep-level transient spectroscopy experiments.

III. RESULTS

A. Perfect-Crystal Y_2O_3

The pseudopotentials have been validated on bulk yttria. Convergence of the total energy to within 10 meV was achieved with a 500 eV cutoff energy for plane wave basis and a Monkhorst-Pack k -point grid of $2 \times 2 \times 2$ for Brillouin zone integration. The calculated parameters, along with experimental values, are shown in Table I. The bulk modulus (B) is obtained by fitting the energy versus volume curve using a fourth-order polynomial.

Table I. The comparison of calculated and experimental properties of yttria.

		u	x	y	z	a	B (GPa)
Ref. 29	exp	-0.0314	0.389	0.150	0.377	10.604	
Ref. 30	exp	-0.0323	0.391	0.150	0.383		
Ref. 31	exp						150
Ref. 32	LDA	-0.0326	0.3907	0.1514	0.3797	10.515	
Ref. 32	GGA	-0.0327	0.3908	0.1516	0.3799	10.700	
Present work	GGA	-0.0324	0.3908	0.1515	0.3798	10.7	150

The electron density of states (DOS), as well as their atomic and orbital resolved DOS, are shown in Fig. 1. It can be seen that a valence band (VB3) of yttrium 4*p* is centered around -20 eV, a valence band (VB2) of oxygen 2*s* is centered around -15 eV, a valence band (VB1) of oxygen 2*p* occurs below 0 eV and a conduction band (CB) of yttrium 4*d* occurs above 4.1 eV. There is a small intermixing of Y 4*d* and O 2*p* states in the valence band near 0 eV, which is consistent with the limited covalence bonding between Y and O atoms. The calculated band gap is about 4.1 eV, which is smaller than the experimental value of 6 eV [33]. The underestimation of the band gap energy value is typical of DFT calculations.

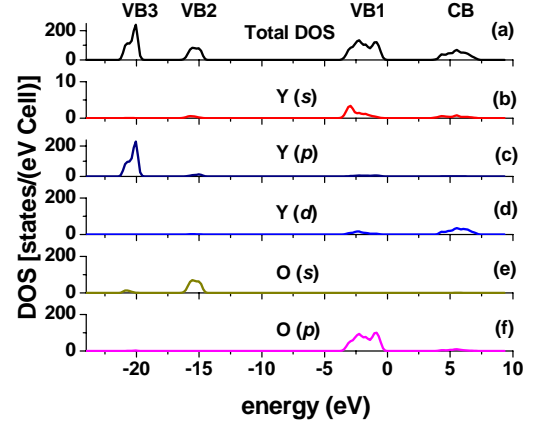


Fig. 1. (a) Total DOS of Y_2O_3 , (b) Y *s*-orbital projected DOS, (c) Y *p*-orbital projected DOS, (d) Y *d*-orbital projected DOS, (e) O *s*-orbital projected DOS, and (f) O *p*-orbital projected DOS.

Table II. Point defect formation energies (E_f) in Y_2O_3 .

Defect	Defect site	Charge on defect	Kröger-Vink notation	$E_f(\mu_Y = \mu_Y^o)$ [eV]		$E_f(\mu_Y = \mu_Y^o + \frac{1}{2}\Delta E_f^{Y_2O_3})$ [eV]	
				$\epsilon_F = 0$ eV	$\epsilon_F = 6$ eV	$\epsilon_F = 0$ eV	$\epsilon_F = 6$ eV
V_o	<i>e</i>	0	V_o^X	0.45	0.45	6.92	6.92
V_o	<i>e</i>	+1	V_o^\cdot	-2.46	3.54	4.01	10.01
V_o	<i>e</i>	+2	$V_o^{\cdot\cdot}$	-5.21	6.79	1.25	13.25
V_Y	<i>b</i>	0	V_Y^X	13.52	13.52	3.82	3.82
V_Y	<i>b</i>	-1	V_Y^\cdot	13.59	7.59	3.89	-2.11
V_Y	<i>b</i>	-2	$V_Y^{\cdot\cdot}$	13.75	1.75	4.05	-7.95
V_Y	<i>b</i>	-3	$V_Y^{\cdot\cdot\cdot}$	14.07	-3.93	4.37	-13.63
O_i	<i>c</i>	0	O_i^X	7.85	7.85	1.38	1.38
O_i	<i>c</i>	-1	O_i^\cdot	8.01	2.01	1.54	-4.46
O_i	<i>c</i>	-2	$O_i^{\cdot\cdot}$	8.38	-3.62	1.91	-10.09
Y_i	<i>c</i>	0	Y_i^X	4.78	4.78	14.48	14.48
Y_i	<i>c</i>	+1	Y_i^\cdot	0.63	6.63	10.33	16.33
Y_i	<i>c</i>	+2	$Y_i^{\cdot\cdot}$	-2.98	9.02	6.72	18.72
Y_i	<i>c</i>	+3	$Y_i^{\cdot\cdot\cdot}$	-6.58	11.42	3.11	21.11
Y_o	<i>e</i>	0	Y_o^X	6.03	6.03	22.20	22.20
Y_o	<i>e</i>	+1	Y_o^\cdot	1.94	7.94	18.10	24.10
Y_o	<i>e</i>	+2	$Y_o^{\cdot\cdot}$	-1.98	10.02	14.19	26.19
Y_o	<i>e</i>	+3	$Y_o^{\cdot\cdot\cdot}$	-6.34	11.66	9.82	27.82
O_Y	<i>d</i>	0	O_Y^X	18.37	18.37	2.20	2.20
O_Y	<i>d</i>	-1	O_Y^\cdot	19.27	13.27	3.10	-2.90
O_Y	<i>d</i>	-2	$O_Y^{\cdot\cdot}$	21.22	9.22	5.05	-6.95

B. Defect formation energies

Yttrium metal has a hexagonal closed packed structure. Using a $20 \times 20 \times 20$ uniform k -space mesh, we calculate equilibrium lattice parameters of $a = 3.63 \text{ \AA}$ (3.65 \AA) and $c = 5.70 \text{ \AA}$ (5.73 \AA). Values in parenthesis are experimental data from Ref. 29. The energy of O_2 was calculated from a single molecule in a 10 \AA cubic cell. While the calculated formation energy for Y_2O_3 of $-19.41 \text{ eV}/Y_2O_3$ is close to the experimental enthalpy of formation of $-19.62 \text{ eV}/Y_2O_3$ [34], this result may be fortuitous given the known issue in calculating the O_2 binding energy.

The energy to form Y-vacancies on the Y1 and Y2 sites are similar. The Y1 vacancy formation energy is about 0.2 eV lower than the Y2 vacancy formation energy; thus only Y1 vacancy formation energies are reported. There are two interstitial sites, $8a$ and $16c$, in yttria. The interstitial site at $8a$ is octahedrally coordinated, surrounded by 6 oxygen atoms and 6 yttrium atoms. The interstitial site at $16c$ is surrounded by 4 yttrium atoms and 6 oxygen atoms and filling it with oxygen would lead to a fluorite structure. The formation energies for interstitials (both oxygen and yttrium) at $8a$ are always 0.4-1.2 eV higher than interstitials at $16c$ site. Thus only formation energies for interstitials at $16c$ are reported. For oxygen antisites, the oxygen at Y2 has 2-3 eV lower energy than the oxygen at Y1; thus the formation energies for oxygen at Y2 site are reported. The formation energies for these defects in various charge states and at the different extremes of chemical potentials and Fermi levels are given in Table II.

The lower limit for the Fermi level ($\epsilon_F = 0 \text{ eV}$) corresponds to the top of the valence band while the upper limit ($\epsilon_F = 6 \text{ eV}$) represents the bottom of the experimental conduction band. The formation energies for different defects as a function of Fermi level for the two limiting yttrium chemical potentials and one intermediate yttrium chemical potential are shown in Fig. 2. The slope of the lines in these figures corresponds to the charge state of the defect. For each defect, the line for a particular charge state has only been drawn over the range where this charge state has the lowest energy of all possible charge states. The changes of slope in the curves correspond to the transitions between charge states (and hence to thermodynamic defect energy levels).

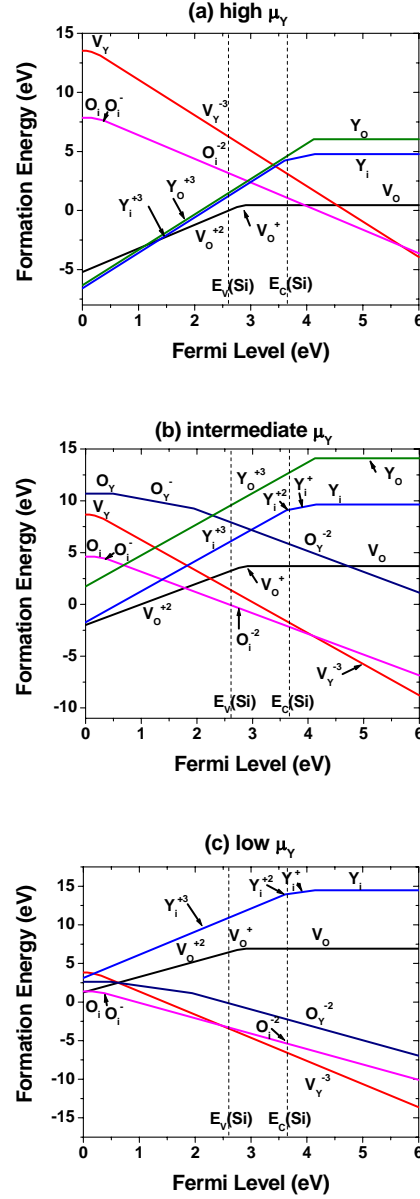


Fig. 2. (Color online) Calculated defect formation energy for native point defects in Y_2O_3 as a function of Fermi level and for (a) $\mu_Y = \mu_Y^o$ (high yttrium partial pressure or low oxygen partial pressure), (b) $\mu_Y = \mu_Y^o + \frac{1}{4} \Delta E_f^{Y_2O_3}$ (intermediate yttrium partial pressure), and (c) $\mu_Y = \mu_Y^o + \frac{1}{2} \Delta E_f^{Y_2O_3}$ (low yttrium partial pressure or high oxygen partial pressure). Only the lowest formation energy values for defects in different charge states are shown. The positions of the valence band maximum ($E_V(\text{Si})$) and conduction band minimum ($E_C(\text{Si})$) of Si with respect to the conduction band minimum of Y_2O_3 are also marked by dashed lines.

C. Defect structure

The results from our calculations suggest that the most common native point defects are oxygen vacancies, oxygen interstitials and yttrium vacancies when Y_2O_3 is used as a gate oxide in MOS devices. We include a summary of relaxed local bond lengths for these defect types in Table III. The changes in bond lengths for each defect can be understood in terms of ionic size and charge effects. When an oxygen atom is removed, nearest yttrium atoms move slightly away from the vacancy site as they are no longer electrostatically attracted to it, and oxygen atoms move closer to the vacancy site as the electrostatic repulsion is reduced. This is different from what is found for oxygen vacancies in ZnO [17] in which nearest zinc atoms move closer to an oxygen vacancy. Near an yttrium vacancy, oxygen atoms move farther away from the vacancy site while yttrium atoms move slightly closer to the vacancy site. This is similar to what was observed for zinc vacancies in ZnO [17]. For the oxygen interstitial, the neighboring yttrium atoms move closer to the interstitial site since they are electrostatically attracted and the neighboring oxygen atoms move away from the interstitial site due to the electrostatic repulsion from the interstitial oxygen.

IV. DISCUSSION

Under high yttrium partial pressure (or low oxygen partial pressure) in Fig. 2(a), Y_i and

V_O are competing defects when the Fermi level is close to the VBM of Y_2O_3 . As the Fermi level moves up, V_O becomes dominant and finally O_i dominates when the Fermi level is close to the CBM. Lowering the yttrium partial pressure from Fig. 2(a) to Fig. 2(b), as the Fermi level changes from the VBM to the CBM, V_O becomes dominant; this is followed by O_i and finally V_Y . Under low yttrium partial pressure in Fig. 2(c), O_i dominates when the Fermi level is close to the VBM and V_Y dominates when the Fermi level is close to the CBM.

The transition Fermi levels for the dominant defect types, V_O , O_i , V_Y and Y_i , are shown in Fig. 3, within the calculated band gap. The transition energies for both oxygen interstitial (O_i) and yttrium vacancy (V_Y) are very close to the VBM of Y_2O_3 , while the transitions for the oxygen vacancy (V_O) are located ~ 1.2 - 1.4 eV below the calculated CBM and that for the yttrium interstitial (Y_i) are located about 0.5 eV below the CBM.

As the band gap of Y_2O_3 is underestimated by 1.9 eV in GGA, it is important to estimate how the thermodynamic transition levels shown in Fig. 3 would change with a more accurate band gap. One common method [17, 23, 35] to include the effect of band gap corrections is to leave the energy levels of the acceptor-like defects near the VBM unchanged, but let the donor-like defects near the CBM shift upward as the band gap is opened up. The DOS plot shown in Fig.1 indicates that the top of the valence band is mainly formed by oxygen $2p$ states while the

Table III. Distances to nearest-neighbor atoms for bulk and defect sites in Y_2O_3 . d_i is the distance of the i th nearest neighbor in angstroms. The values in parentheses are the number of neighbors having the same distance.

	Neighbor type	d_1	d_2	d_3	d_4
O (in bulk Y_2O_3)	Y	2.27	2.29	2.30	2.36
	O	2.94(2)	2.95(2)		
Neutral V_O	Y	2.29	2.35	2.36	2.39
	O	2.903	2.907	2.91	2.92
Y (in bulk Y_2O_3)	Y	3.55(6)			
	O	2.30(6)			
Neutral V_Y	Y	3.53(6)			
	O	2.61(6)			
O (before relaxation)	Y	2.47(3)	2.50		
	O	2.43(3)	2.50(3)		
Neutral O_i	Y	2.30	2.34(3)		
	O	2.61(3)	2.65(3)		

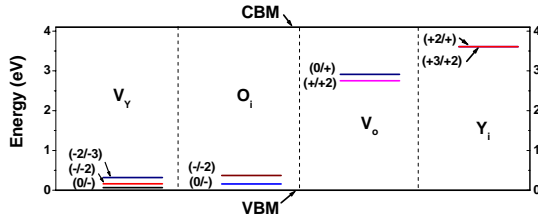


Fig. 3. The position of the thermodynamic transition energy levels in the calculated band gap (4.1 eV) of Y_2O_3 .

bottom of the conduction band is composed of yttrium $4d$ states. Thus the defect states derived from oxygen $2p$ states exhibit valence-band character while the defect states derived from yttrium $4d$ states have conduction-band character.

The neutral oxygen vacancy (V_O) removes 3 states and four $2p$ electrons from the top of the valence band. As a result, two electrons have to occupy conduction-band-like states which are pulled into the gap by the oxygen vacancy. Thus the defect states from oxygen vacancies exhibit conduction-band character. The formation energy of the neutral oxygen vacancy may shift to a higher value if the conduction band were to be moved up from the calculated value since there are two electrons in this defect level. The formation energy of V_O^{2+} will remain unchanged since this defect level is empty. Therefore, the thermodynamic transition energy levels $+2/+1$ and $+1/0$ for oxygen vacancies may move upwards. Since one yttrium interstitial does not add additional states to the top of the valence band, new states are created in the band gap to accommodate three electrons ($5s^24d^1$). Thus the defect states from yttrium interstitials also exhibit conduction-band character.

On the other hand, one neutral yttrium vacancy does not change the number of states in the top of the valence band, but it removes three electrons from the top of the valence band. Thus, the defect levels from yttrium vacancies exhibit more valence-band character. An oxygen interstitial adds three $2p$ states to the top of the valence band and thus also exhibits more valence-band character. The thermodynamic transition energy levels from both defects (i.e., yttrium vacancies and oxygen interstitials) are likely to be only slightly affected by a band gap correction.

Based on the discussion above, we can investigate the effect of the defect levels on the

operation of devices based on Y_2O_3 gate oxides. When Y_2O_3 is used as a gate insulator material in MOS devices, the electron reservoir to form a charged defect comes from the polysilicon gate or silicon substrate. This limits the range for the electron chemical potential to be between the valence band maximum and the conduction band minimum of Si, which is 2.3 - 3.4 eV below the conduction band minimum of Y_2O_3 [33]. Under high yttrium chemical potential (or low oxygen partial pressure) in Fig. 2(a), the dominant defect types in this range of electron chemical potential are oxygen vacancies. Under intermediate yttrium chemical potential (Fig. 2(b)), charged oxygen interstitials become dominant. Under low yttrium chemical potential (or high oxygen partial pressure) (Fig. 2(c)), charged yttrium vacancies are dominant. The defect levels from oxygen interstitials and yttrium vacancies are close to the VBM of Y_2O_3 and will be negatively charged in most of the range of the electron chemical potential. Thus they will only contribute to the negative fixed charge. However, the defect levels from oxygen vacancies will move upwards when the band gap correction is applied. They may become positively charged and act as electron traps. It was generally found from experiment that there are pre-existing defects which generate positive fixed charge and electron traps in the Y_2O_3 film [8-10]. The positive fixed charge will shift the flatband voltage while the electron traps can cause threshold voltage instabilities. Therefore, based on our results, we suggest that the film should be grown under low to intermediate yttrium partial pressure to suppress the oxygen vacancy formation.

V. CONCLUSIONS

A first-principles study of point defects in Y_2O_3 has been carried out. We find that oxygen vacancies are the dominant defect types under high yttrium chemical potential condition. Lower yttrium chemical potential leads to oxygen interstitials and ultimately yttrium vacancies when Y_2O_3 is used as a high-k gate oxide material in MOS devices. The oxygen vacancies have transition levels near the conduction band and may be responsible for the positive fixed charges and electron traps observed in experiments.

ACKNOWLEDGEMENTS

The authors would like to thank the Singapore-MIT Alliance and the National University of Singapore for supporting this work. T. Maxisch acknowledges the support by the Department of Energy under Contract No. DE-FG02-96ER45571 and by the MRSEC program of the National Science Foundation under Contract No. DMR-0213282. Additional computing resources were provided by the National Science Foundation, National Partnership for Advanced Computing Infrastructure (NPACI).

REFERENCES

- [1] R. McKee, F. Walker and M. Chisholm, "Crystalline oxides on silicon – alternative dielectrics for advanced transistor technologies", *Mat. Res. Soc. Symp. Proc.*, 567, 415-425, 1999.
- [2] G.D. Wilk, R.M. Wallace and J.M. Anthony, "High-k gate dielectrics: Current status and materials properties considerations", *J. Appl. Phys.*, 89 (10), 5243-5275, 2001.
- [3] E. P. Gusev, E. Cartier, D. A. Buchanan, M. Gribelyuk, M. Copel, H. Okorn-Schmidt, and C. D'Emic, "Ultrathin high-k metal oxides on silicon: processing, characterization and integration issues", *Microelectronic Engineering*, 59(1-4), 341-349, 2001.
- [4] J. Kwo, M. Hong, A. R. Kortan, K. L. Queeney, Y. J. Chabal, J. P. Mannaerts, T. Boone, J. J. Krajewski, A. M. Sergent, and J. M. Rosamilia, "High ϵ gate dielectrics Gd₂O₃ and Y₂O₃ for silicon", *Appl. Phys. Lett.*, 77(1), 130-132, 2000.
- [5] J. Kwo, M. Hong, A. R. Kortan, K. L. Queeney, Y. J. Chabal, R. L. Opila, D. A. Muller, S. N. G. Chu, B. J. Sapjeta, T. S. Lay, J. P. Mannaerts, T. Boone, H. W. Krautter, J. J. Krajewski, A. M. Sergent, and J. M. Rosamilia, "Properties of high k gate dielectrics Gd₂O₃ and Y₂O₃ for Si", *J. Appl. Phys.*, 89(7), 3920-3927, 2001.
- [6] S. Guha, E. Cartier, M. A. Gribelyuk, N. A. Bojarczuk, and M. C. Copel, "Atomic beam deposition of lanthanum- and yttrium-based oxide thin films for gate dielectrics", *Appl. Phys. Lett.*, 77 (17), 2710-2712, 2000.
- [7] L.-A. Ragnarsson, S. Guha, M. Copel, E. Cartier, N. A. Bojarczuk, and J. Karasinski, "Molecular-beam-deposited yttrium-oxide dielectrics in aluminum-gated metal-oxide-semiconductor field-effect transistors: Effective electron mobility", *Appl. Phys. Lett.*, 78(26), 4169, 2001.
- [8] E. K. Evangelou, C. Wiemer, and M. Fanciulli, M. Sethu and W. Cranton, "Electrical and structural characteristics of yttrium oxide films deposited by rf-magnetron sputtering on n-Si", *J. Appl. Phys.*, 94(1), 318-325, 2003.
- [9] Rastogi AC, Desu SB, "Current Conduction and Dielectric Behavior of High k-Y₂O₃ Films integrated with Si Using Chemical Vapor Deposition as a Gate Dielectric for Metal-Oxide-Semiconductor Devices", *J. Electroceramics*, 13, 121-127, 2004.
- [10] Rastogi A. C., Sharma R. N., "Interfacial charge trapping in extrinsic Y₂O₃/SiO₂ bilayer gate dielectric based MIS devices on Si(100)", *Semicond. Sci. Technol.*, 16, 641-650, 2001.
- [11] F. Jollet, C. Noguera, N. Thommat, M. Gautier, and J. -P. Duraud, "Electronic structure of yttrium oxide", *Phys. Rev. B*, 42 (12), 7587-7595, 1990.
- [12] F. Jollet, C. Noguera, M. Gautier, N. Thommat, and J. -P. Duraud, "Influence of oxygen vacancies on the electronic structure of yttrium oxide", *J. Am. Ceram. Soc.*, 74(2), 358-364, 1991.
- [13] D. R. Mueller, D. L. Ederer, J. vanEk, W. L. O'Brien, Q. Y. Dong, J. J. Jia, and T. A. Callcott, "Soft-x-ray emission and the local p-type partial density of electronic states in Y₂O₃: experiment and theory", *Phys. Rev. B*, 54(21), 15034-15039, 1996.
- [14] Y. N. Xu, Z. Q. Gu and W. Y. Ching, "Electronic, structural and optical properties of crystalline yttria", *Phys. Rev. B*, 56, 14993-15000, 1997.
- [15] G. Kresse and J. Hafner, *Phys. Rev. B* 47, 558 (1993); G. Kresse and J. Furthmuller, *Phys. Rev. B* 54, 11169 (1996).
- [16] G. Kresse, and J. Joubert, "From ultrasoft pseudopotentials to the projector augmented wave method", *Phys. Rev. B*, 59, 1758, 1999.
- [17] A. F. Kohan, G. Ceder, and D. Morgan, "First-principles study of native point defects in ZnO", *Phys. Rev. B*, 61, 15019-15027, 2000.
- [18] S. B. Zhang, S.-H. Wei, and A. Zunger, "Intrinsic n-type versus p-type doping asymmetry and the defect physics of ZnO", *Phys. Rev. B*, 63, 075205, 2001.
- [19] D. B. Laks, C. G. Van de Walle, G. F. Neumark, P. E. Blochl, and S. T. Pantelides, "Native defects and self-compensation in ZnSe", *Phys. Rev. B*, 45, 10965-10978, 1992.
- [20] A. Garcia, and J. E. Northrup, "Compensation of p-type doping in ZnSe: the

- role of impurity-native defect complexes”, *Phys. Rev. Lett.*, 74, 1131-1134, 1995.
- [21] S. Poykko, M. J. Puska, and R. M. Nieminen, “Ab initio study of fully relaxed divacancies in GaAs”, *Phys. Rev. B*, 53, 3813-3819, 1996.
- [22] K. W. Kwak, D. Vanderbilt, and R. D. King-Smith, “First-principles study of phosphorus and nitrogen impurities in ZnSe”, *Phys. Rev. B*, 52, 11912-11919, 1995.
- [23] C. G. Van de Walle, and J. Neugebauer, “First-principles calculations for defects and impurities: applications to III-nitrides”, *J. Appl. Phys.*, 95, 3851-3879, 2004.
- [24] A. Baldereschi, S. Baroni, and R. Resta, “Band offsets in lattice-matched heterojunctions: a model and first-principles calculations for GaAs/AlAs”, *Phys. Rev. Lett.*, 61, 734-737, 1988.
- [25] M. Peressi, N. Binggeli, and A. Baldereschi, “Band engineering at interfaces: theory and numerical experiments”, *J. Phys. D: Appl. Phys.*, 31, 1273-1299, 1998.
- [26] G. Makov, and M. C. Payne, “Periodic boundary conditions in ab initio calculations”, *Phys. Rev. B*, 51(7), 4014, 1995.
- [27] Clas Persson, Y. J. Zhao, S. Lany, and A. Zunger, *Phys. Rev. B*, 035211, 2005.
- [28] J. H. Shim, E. K. Lee, Y. J. Lee and R. M. Nieminen, *Phys. Rev. B*, 035206, 2005.
- [29] R.W.G. Wyckoff, *Crystal Structures* (Wiley, New York), 1963.
- [30] H. Ishibashi, K. Shimomoto and K. Nakahigashi, “Electron density distribution and chemical bonding of Ln_2O_3 (Ln=Y, Tm, Yb) from powder X-ray diffraction data by the maximum-entropy method”, *J. Phy. Chem. Sol.*, 55, 809-814, 1994.
- [31] Ö. Ünal and M. Akinc, “Compressive properties of yttrium oxide”, *J. Am. Ceram. Soc.*, 79, 805-808, 1996.
- [32] L. Marsella, and V. Fiorentini, *Phys. Rev. B*, 69, 172103, 2004.
- [33] J. Robertson, “Band offsets of wide-band-gap oxides and implications for future electronic devices”, *J. Vac. Sci. Tech. B*, 18(3), 1785-1791, 2000.
- [34] J. G. Speight, *Lange’s Handbook of Chemistry*, 16th ed. (McGraw-Hill, New York, 2005).
- [35] S. B. Zhang, S. H. Wei, and A. Zunger, *Phys. Rev. B*, 57(16), 9642, (1998).